High Q^2 π^0 electroproduction in the resonance region

M. Ungaro, K. Joo

February 8, 2023

Abstract

We report the analysis of exclusive single π^0 electroproduction in the resonance region at Jefferson Lab in the Q^2 range $2 \rightarrow 6$ GeV^2. π^0 c.m. angular distributions are obtained over the entire 4 π c.m. solid angle. The c.m. differential cross sections and beam spin asymmetries are measured.

Contents

1 Electron identification

In CLAS electro-production experiments the scattered electron defines the timing of each event, so it is particularly important to make sure that their identification is correct and that there is no contamination from particles such as π^-.

We consider *candidate electrons* every negative track that produced an hardware trigger (this trigger condition is ensured by choosing the first entry in the EVNT bank). The track is also required to have hit matches in the CLAS Čerenkov (CC)[9], Drift Chambers (DC)[6], Electromagnetic Calorimeter (EC)[8] and Time of Flight (SC or TOF)[11], and to have time-based reconstruction (positive DC status word in DCPB).

Starting from a candidate electron, we use the following studies, detailed in the following sections, to defined good electron:

- CC θ, ϕ and time matching in the detector
- EC Threshold
- EC Sampling Fraction
- Track Coordinates in the EC plane
- Minimum Ionizing Particles rejection in the EC
- Electromagnetic Shower Shape in the EC
- *Number of photo-electrons (nphe) in the CC This cut is not used anymore for identification, but the distributions will be shown for comparison with other analyses of e16 data*

For each individual cut we will show four histograms to illustrate its impact:

a. Variable distribution when no cut at all is applied.

b. Variable distribution when all other pid cuts but this one are applied: this helps refining cut parameters. For example, when looking at the sampling fraction, applying all other cuts to helps clean up the plot and to better estimate the sampling fraction cut. We also refer as "calorimeter cuts" all cuts but the *nphe* and EC threshold.

c. Variable distribution all the pid cuts are reversed: these should be particles other than electrons. This condition can help identifying possible contamination.

d. Variable distribution when all cuts, including the one under study, are applied.

The statistics and effectiveness of each case is reported in the plots. Only the relevant plots are reported here. The complete set of plots and projection can be found on the web at: https://userweb.jlab.org/∼ungaro/mauripage/html/projects/pi0/analysis/epid.html.

1.1 CC theta Matching

This, and the following CC ϕ and Time Matching procedures, are based on a study [3],[4], [5] of the Čerenkov response function.

The CC θ matching requires the candidate electrons tracks to match a signal in the CC. The CC segments (one pmt from the right and the corresponding from the left, constitute a segment) and mirrors are placed along the CLAS polar angle. Since the torus magnetic field bend the electrons toward the beamline, it's convenient not to use the track θ angle at the vertex but the angle θ_{CC} of the point of intersection of the track with the CC plane. These are the details of the θ_{CC} calculation:

1. The intersection of the track with the TOF plane $\vec{P}_0$ is considered (DCPB bank).
2. The normalized direction of the track $\vec{n}$ of the track to the TOF plane is considered (DCPB bank).
3. The line representing the un-bending track is then $\vec{P} = \vec{P}_0 - t\vec{n}$ (the minus sign accounts for the fact that the CC is before the TOF).
4. The CC plane equation is considered: $Ax + By + Cz + D = 0$, with $A = -0.000784$, $B = 0$, $C = -0.00168$, and $D = 1$ [3]. This is also represented by the vector $\vec{S} = (A, B, C)$
5. Substituting the line equation in the plane equation one finds the distance of the path length from the intersection of the track with the TOF plane and the intersection of the track with the CC plane:

$$t = \frac{\vec{S} \cdot \vec{P}_0}{\vec{S} \cdot \vec{n}}$$

There should be one to one correspondence between θ_{CC} and segment number for real tracks, while background noise and accidentals should show no such correlation. For each segment, the θ_{CC} distribution is fitted with a gaussian + second order polynomial distribution to determine its mean and width. Examples of these fits can be found in Fig. 1. Events that have $\mu - 4\sigma < \theta_{CC} < \mu - 3\sigma$ pass the cut (this accounts for the distribution not being completely symmetric around the mean). The overall θ_{CC} versus segment distribution and the lower/upper limits are shown in Fig. 2.

There are two exception to this cut:

1. The first and last segments distributions is hard to fit. The cut in this case is ignored.
2. If both (left and right) photomultipliers have a signal the track is kept.

The events that fall in this category can be seen in the bottom right panel in Fig. 2.

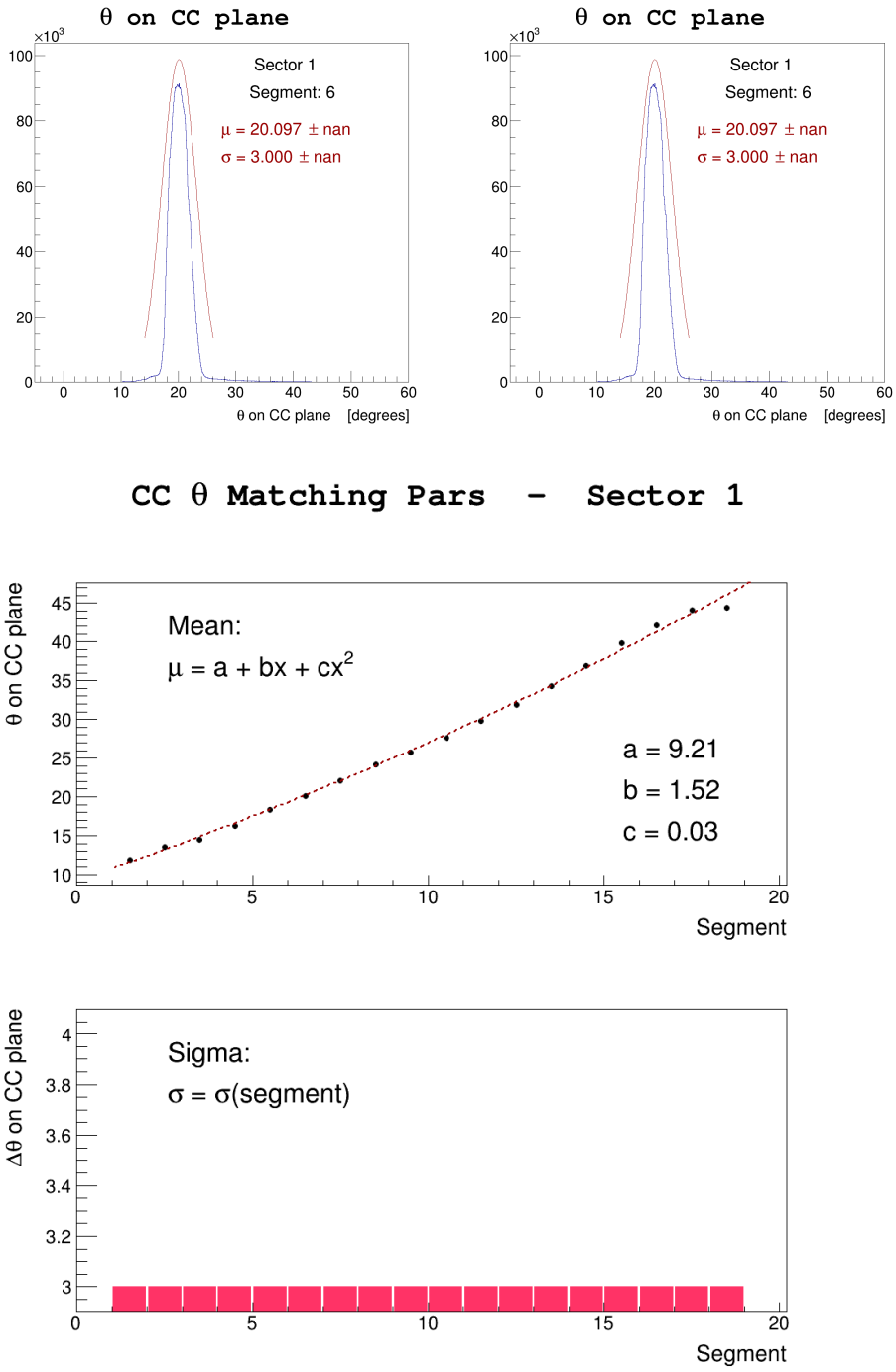

Figure 1: Top panels: θ_{CC} for two segments in sector 1, and gaussian + second order polynomial fit. The distribution is slightly asymmetric to the left, so the lower limit was 4σ while the upper limit was 3σ. Bottom Panels: the mean distribution is fitted with a third order polynomial.

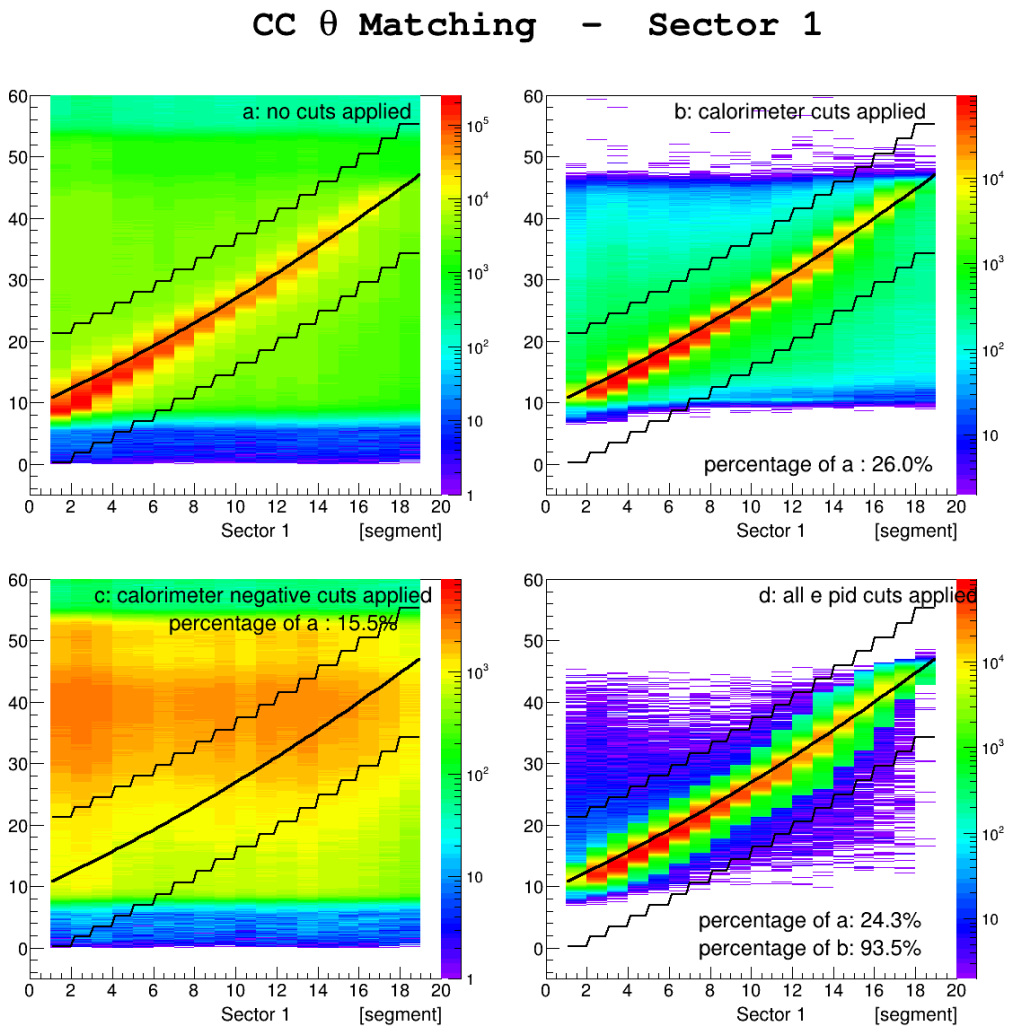

Figure 2: θ_{CC} versus Segment for Sector 1. The θ_{CC} distribution for each segment is fitted with a gaussian + second order polynomial distribution to determine its mean and width. Events that have $\mu - 4\sigma < \theta_{CC} < \mu - 3\sigma$ pass the cut. Top left: all events. Top right: events with calorimeter cuts applied (notice that these cuts remove 74 % of the data). Bottom left: events with the negative calorimeter cuts applied. Bottom right: all cuts applied. Notice that the CC matching cut only removes 7 % of the events with the calorimeter cuts already applied.

1.2 CC phi Matching

The principle of this cut is very simple: when the track is on the right of the CC, the right photo-multiplier should fire, and viceversa. Exception: when ϕ (relative to the center in each sector) is less than 4^0 the track is kept (the Čerenkov light should hit both pmts, but with less efficiency since it splits in the middle)[3],[4], [5].

To show the effects of this cut the quantity "ϕ matching" is plotted in Fig. 3. This quantity is 0 when both pmts are fired, $1(-1)$ when there is a left (right) match and $2(-2)$ there is a left (right) mismatch. The cut applied is: "ϕ matching"< 2 except when $|\phi| < 4^0$.

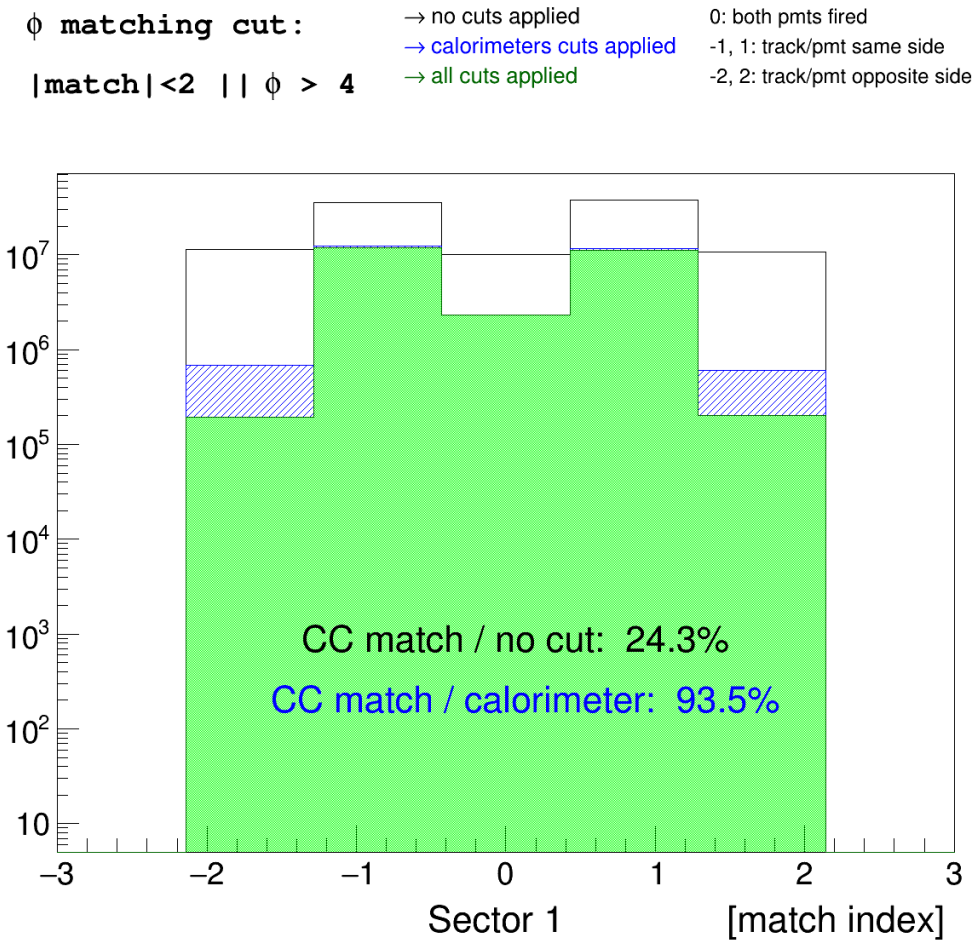

Figure 3: "ϕ matching": this quantity is 0 when both pmts are fired, $1(-1)$ when there is a left (right) match and $2(-2)$ there is a left (right) mismatch. The cut applied is: "ϕ matching"< 2 except when $|\phi| < 4^0$.

1.3 CC time Matching

The CC timing was not calibrated in e1-6, but a timing cut is still possible if applied to each tube (this is basically equivalent to perform the timing calibration).

The difference ΔT between the track time recorded on a CC segment and corresponding time recorded on the TOF, corrected for the path length from the CC to the TOF, is fitted with a gaussian (see Fig. 4). Since there could be multiple Čerenkov light reflections leading to a time delay, a 3 sigma cut is applied on the *left* of the signal, and not on the right. This difference is plotted in Fig. 5 for all tubes in sector one.

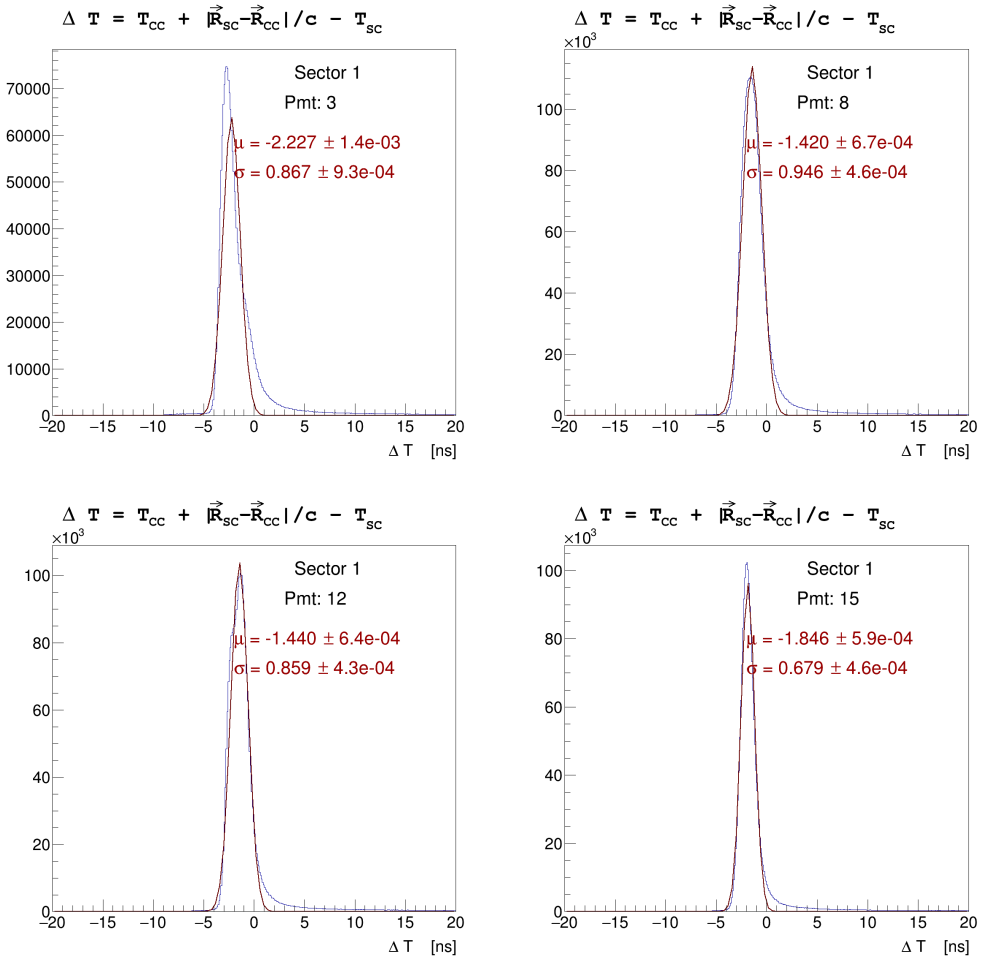

Figure 4: CC time matching. The difference ΔT between the track time recorded at a CC tube (T_{CC}) and corresponding time recorded on the TOF (T_{SC}), corrected for the path length from the CC to the TOF ($|\vec{R_{CC}} - \vec{R_{SC}}|/c$), shown here for 4 CC pmts, is fitted with a gaussian. A 5σ cut is applied on the left of the signal.

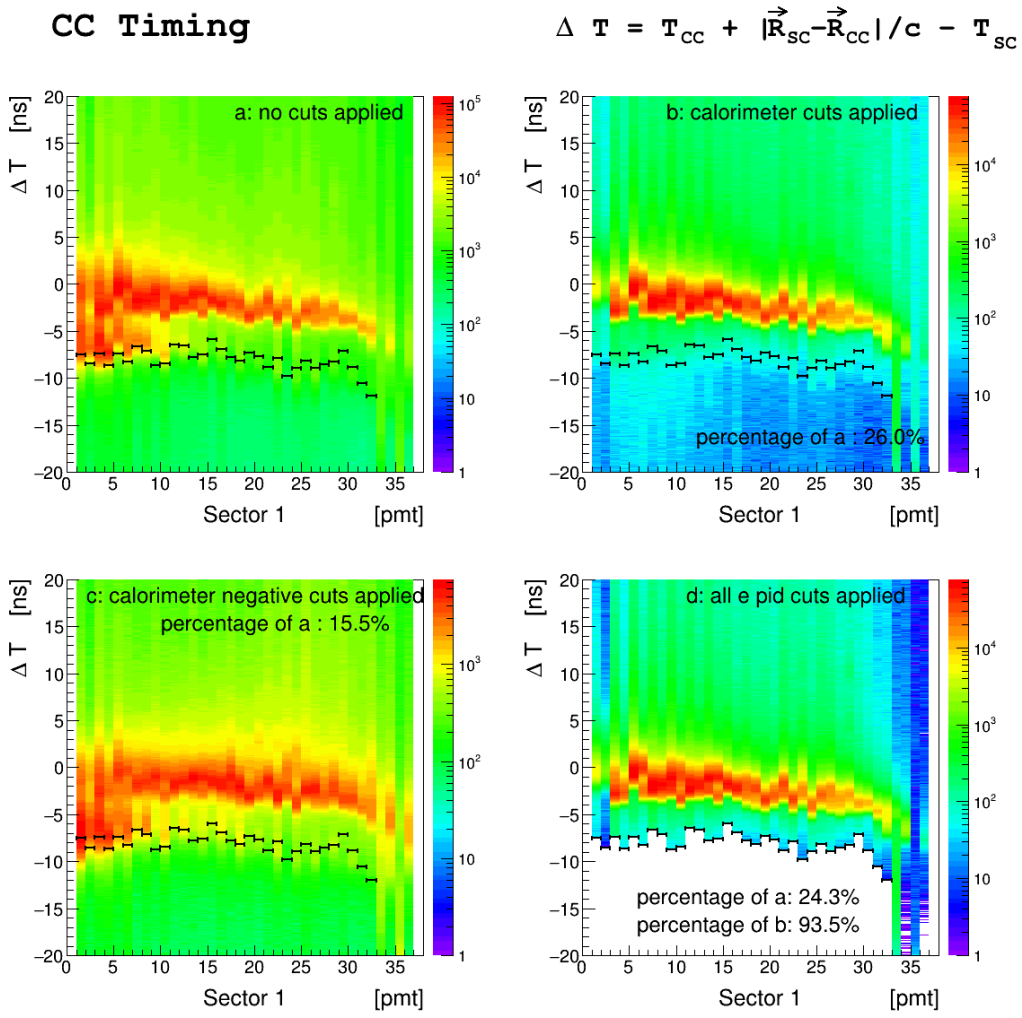

Figure 5: CC time matching. The difference ΔT between the track time recorded at a CC tube (T_{CC}) and corresponding time recorded on the TOF (T_{SC}), corrected for the path length from the CC to the TOF ($|\vec{R_{CC}} - \vec{R_{SC}}|/c$), is fitted with a gaussian. A 3σ cut is applied on the left of the signal. Top left: all events. Top right: events with calorimeter cuts applied. notice that these cuts remove 71 % of the data. Bottom left: events with the negative calorimeter cuts applied. Bottom right: all cuts applied. Notice that the CC matching cut only removes 7 % of the events with the calorimeter cuts already applied.

1.4 EC Threshold

A study [1] of the inclusive cross section at various beam energies in CLAS results in a parametrization of the low momentum cut p_{min} as a function of the calorimeter low total threshold (in milliVolts) of the trigger discriminator:

$$p_{min}\ (\text{MeV}) = 214 + 2.47 \times EC_{threshold}(\text{mV}) \tag{1}$$

The low total threshold for e1-6 was 172 mV therefore the minimum momentum cut is fixed at:

$$p_{min} = 0.64\ \text{GeV}$$

Fig. 6 shows for the momentum distribution of the candidates integrated over all sectors. In average, $\sim$ 27.7% pass the all other particle ID cuts and of these, 91.9% pass the minimum p cut.

The cut value used is the same for all sectors and its effectiveness is summarized in table 1.4.

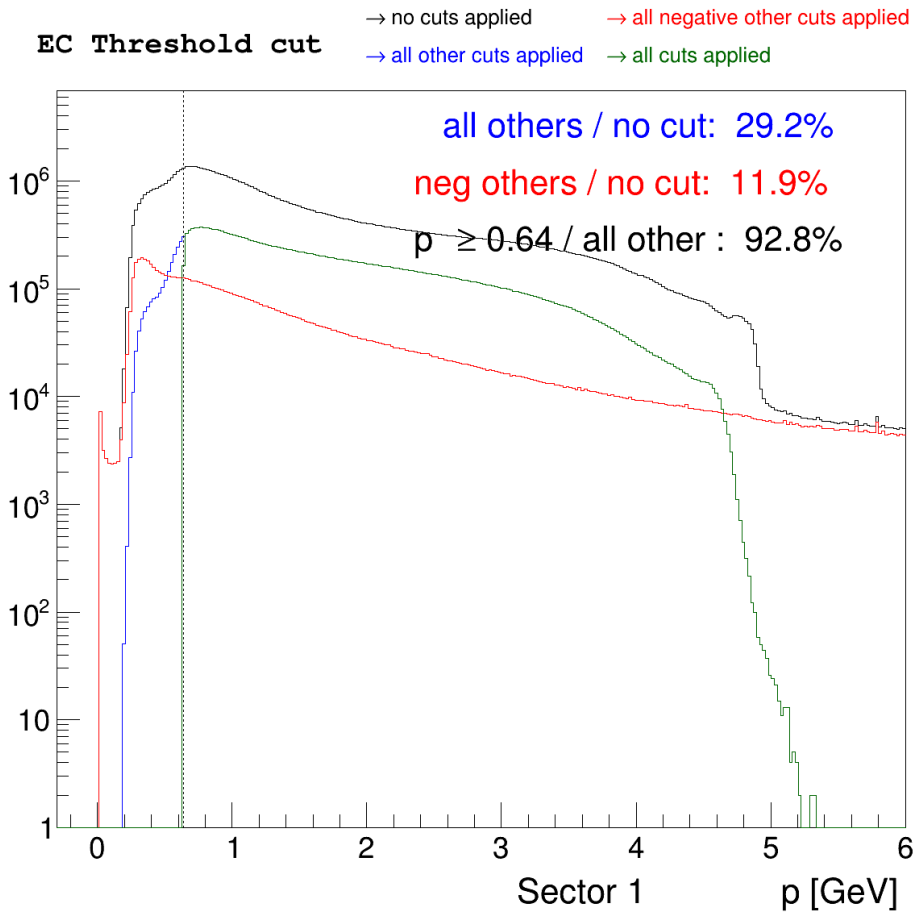

Figure 6: Candidates Momentum distribution in each sector. The minimum momentum cut is chosen according to Eq.1. In average, $\sim$ 82 % of the candidates have a signal in the EC. Of those, 30 % pass the all other particle ID cuts and of these, 92.5 % pass the minimum p cut.

Sector	all other cuts GeV	minimum p cut %	
1	71.1	93.1	
2	72.1	89.8	
3	71.9	91.6	
4	71.8	93.7	
5	75.2	90.0	
6	72.6	92.8	

Table 1: The minimum p cut values and effectiveness in each sector. The last column refers to events with signal in EC that pass the minimum p cut.

1.5 EC Sampling Fraction

When going through the EC calorimeter, in the momentum range of particles detected in CLAS, charged pions are minimum ionizing particles, while electrons shower with a total energy deposition E_{tot} proportional to their momentum p. Therefore the sampling fraction E_{tot}/p should be independent of momentum (in reality there is a slight dependence).

The total energy in the calorimeter E_{tot} is not always calculated to be the sum of the energies in the inner and outer part of the calorimeter E_{in} and E_{out}, due to wrong calculation/comparison with the DC momentum [2]. In this analysis we recalculated E_{tot} as $E_{in} + E_{out}$ when that happened, by taking the larger between E_{tot} and $E_{in} + E_{out}$.

After applying all the other electron ID cuts, the sampling fraction is plotted in each sector as a function of momentum (see Fig. 7). The plot is divided in 15 momentum slices and each slice is fitted with a gaussian + second order polynomial function. The final result is a $3rd$ order polynomial function that parametrizes the mean and the sigma of the sampling fraction as a function of p. Since the negative pions in this plot would be below the electrons, the cut chosen is not exactly symmetric around the mean, but looser on the upper part: upper: 3.4σ; lower: 3σ.

In Fig. 8 the Sampling Fraction for sector 1 is plotted for no cuts, all other cuts, all other negative cuts and all cuts respectively. One can see that all the other cuts result in a quite good selection already, and that the sampling fraction cut (d) keeps $\sim 90\%$ of those events.

In Fig. 9 a comparison of the sampling fraction in all sectors is shown. The cut values used in each sector and their effectiveness are summarized in table 1.5. The parameters used are listed in sec.1.5.1.

Sector	events with EC GeV	SF cut %	%
1	73.8	60.1	
2	74.7	59.0	
3	75.6	57.5	
4	73.0	58.5	
5	74.9	60.3	
6	75.0	58.5	

Table 2: The Sampling Fraction (SF) cut values and effectiveness in each sector. The second column refers to events with signal in EC that pass the SF cut.

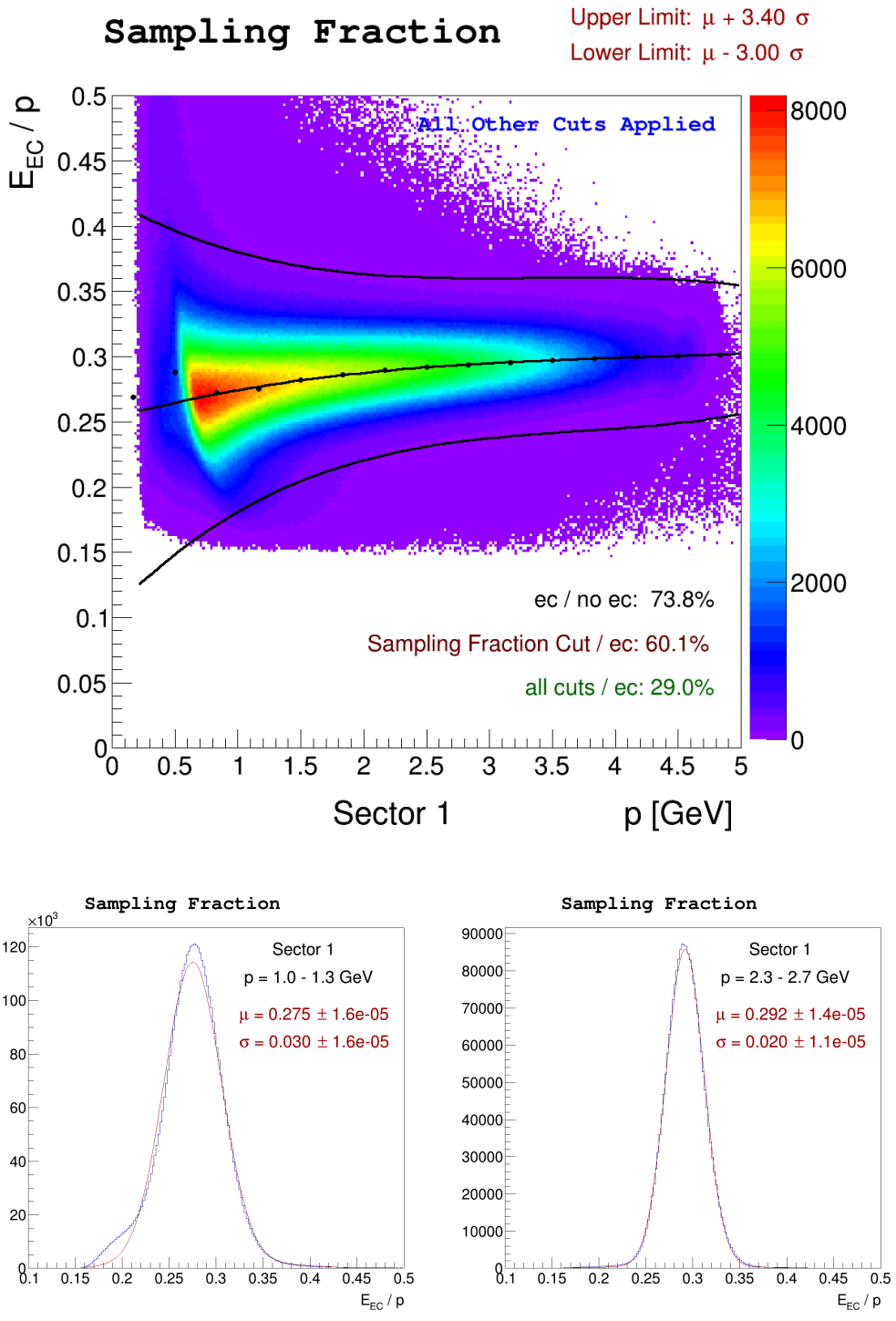

Figure 7: Top: Sampling Fraction as a function of momentum for Sector 1. Bottom: four momentum slices, and gaussian + second order polynomial fit. The number of sigmas that define the cut are: upper: 3.4σ; lower: 3σ.

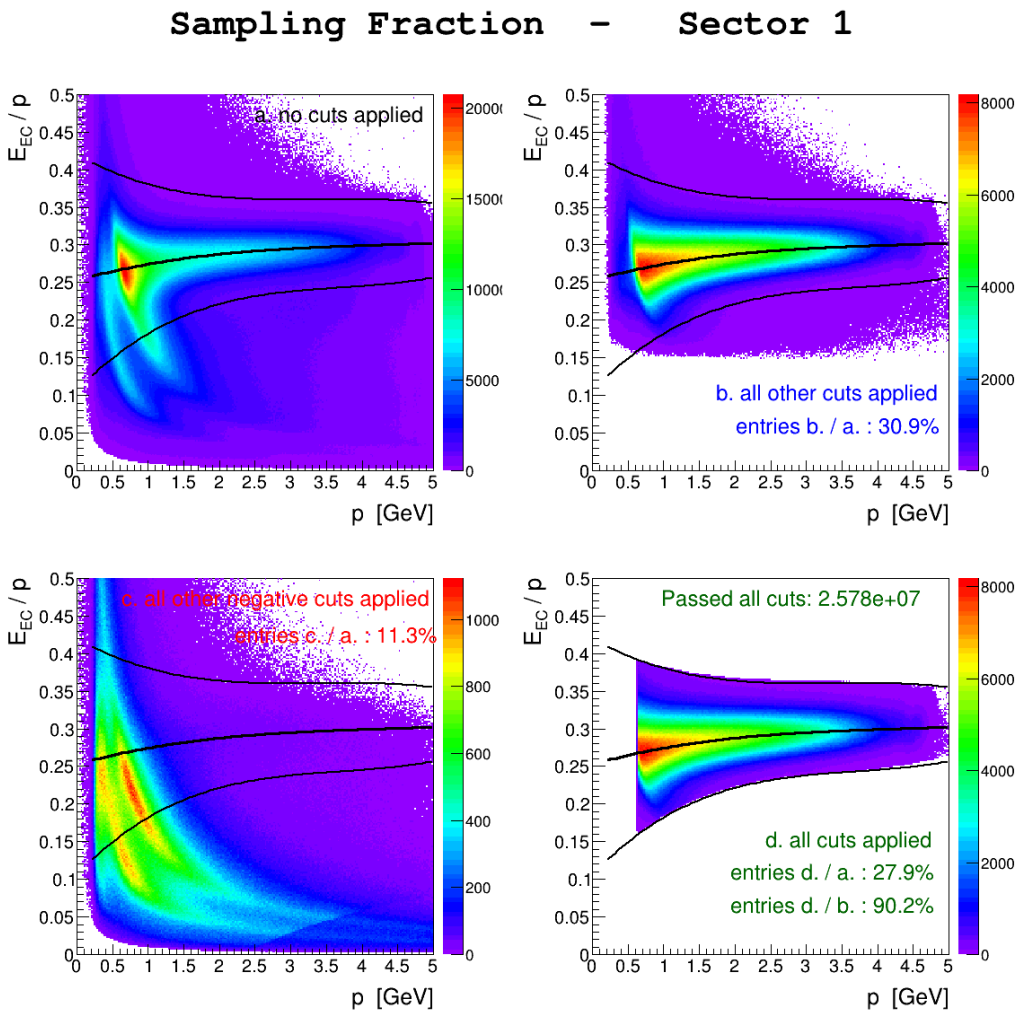

Figure 8: Sampling Fraction cut. Notice in panel (b) all the other cuts but the sampling fraction applied; the sampling fraction cut (d) keeps 90.5 % of the events in panel (b).

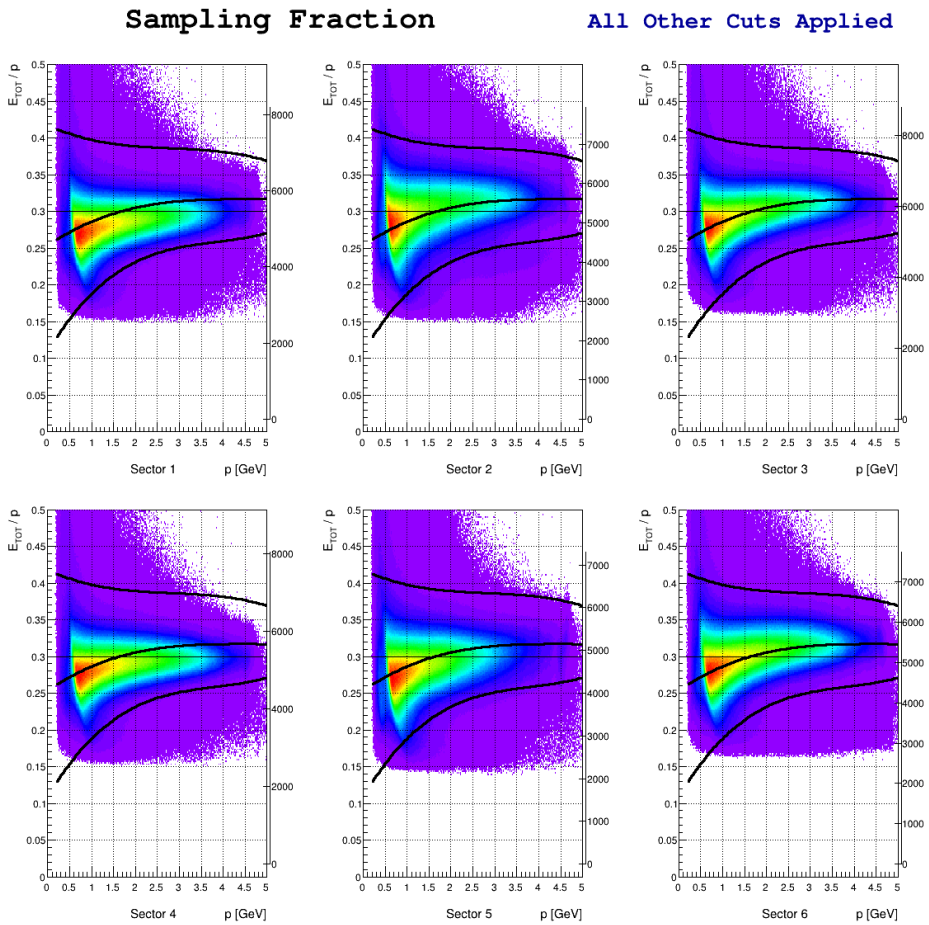

Figure 9: Sampling Fraction cut in all sectors. Plot grid and the line at 0.3 emphasize differences between sectors.

1.5.1 Cut parameters

$$f(p) = a + bp + cp^2 + dp^3$$

	S1	S2	S3	S4	S5	S6
mean:						
a:	0.249471	0.252591	0.250881	0.246831	0.247017	0.248919
b:	0.0350377	0.0487858	0.0443294	0.0381502	0.0326401	0.0467523
c:	-0.00887004	-0.0130587	-0.0101895	-0.00993875	-0.00788004	-0.0110489
d:	0.000827307	0.00120111	0.000785888	0.000882525	0.000684981	0.000902679
sigma						
a:	0.0482422	0.0501838	0.0483883	0.0435729	0.0463011	0.0452695
b:	-0.0234008	-0.0206365	-0.0243889	-0.018439	-0.0173496	-0.0180503
c:	0.00652057	0.00521743	0.00709145	0.00486129	0.00460028	0.00473553
d:	-0.000643782	-0.000504944	-0.000731488	-0.000498339	-0.00041353	-0.000477848

1.6 Track Coordinates in the EC plane

The EC is designed for the electron to release all their energy in it. However electrons that shower near the edges of the calorimeter will not loose all their energy in the detector because the shower is not fully contained, thus their energy cannot be properly reconstructed. For this reason a fiducial cut is introduced on the track coordinates U, V, W of the electrons at the EC plane. The U, V, W coordinates are chosen for convenience since they are parallel to the directions of the EC scintillators (and to the EC edges). The cuts have been adjusted by looking at Fig. 3 and making sure the distribution is ϕ-symmetric

$$40 \leq U \leq 400, V \leq 362, W \leq 395$$

The U, V, W distributions are plotted in Fig. 10,11,12, respectively. In average 80.9% of all the events with an EC signal pass the U cut, 71.3% the V cut and 69.4% the W cut, for a combined pass/total ratio of 58%. When all other cuts are applied the U,V,W keep 96.6%, 88.6%, 86.8% events respectively, for a combined effective cut of 77.8% (the product of these numbers is 74.2% but the corners events are correlated).

In Fig. 13 is plotted the Y versus X track coordinate in the EC plane before and after the U, V, W cuts.

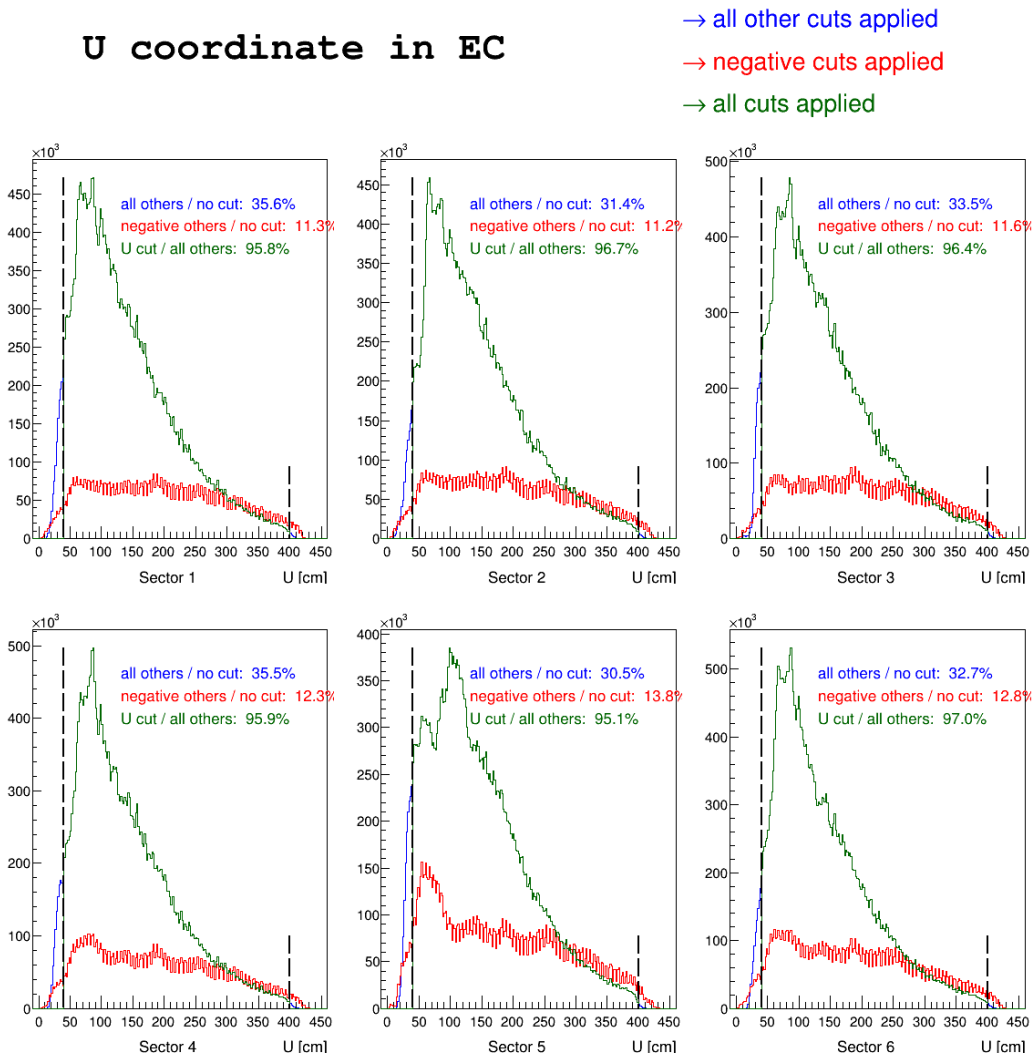

Figure 10: U track coordinate in the EC plane for all sectors. The cut is chosen to avoid edge effects that truncate the electron shower.

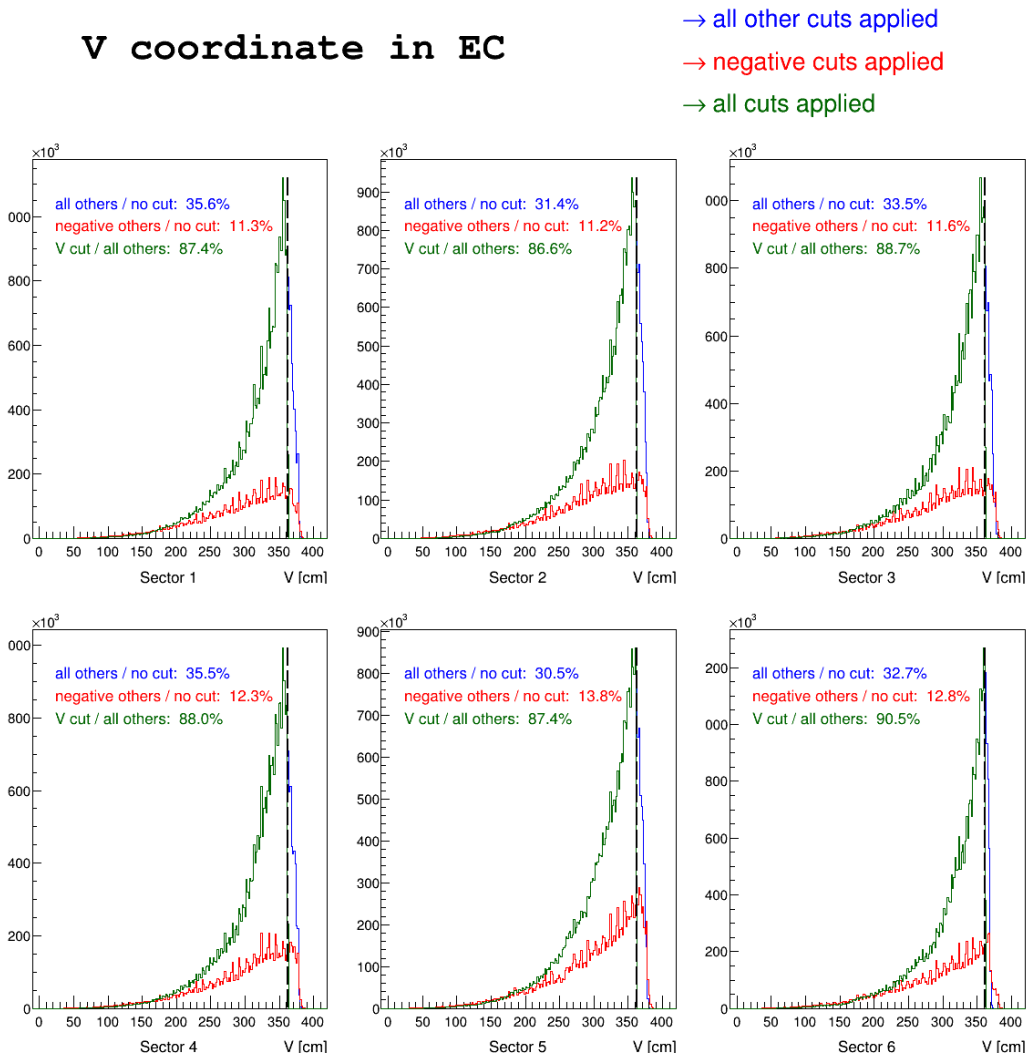

Figure 11: V track coordinate in the EC plane for all sectors. The cut is chosen to avoid edge effects that truncate the electron shower.

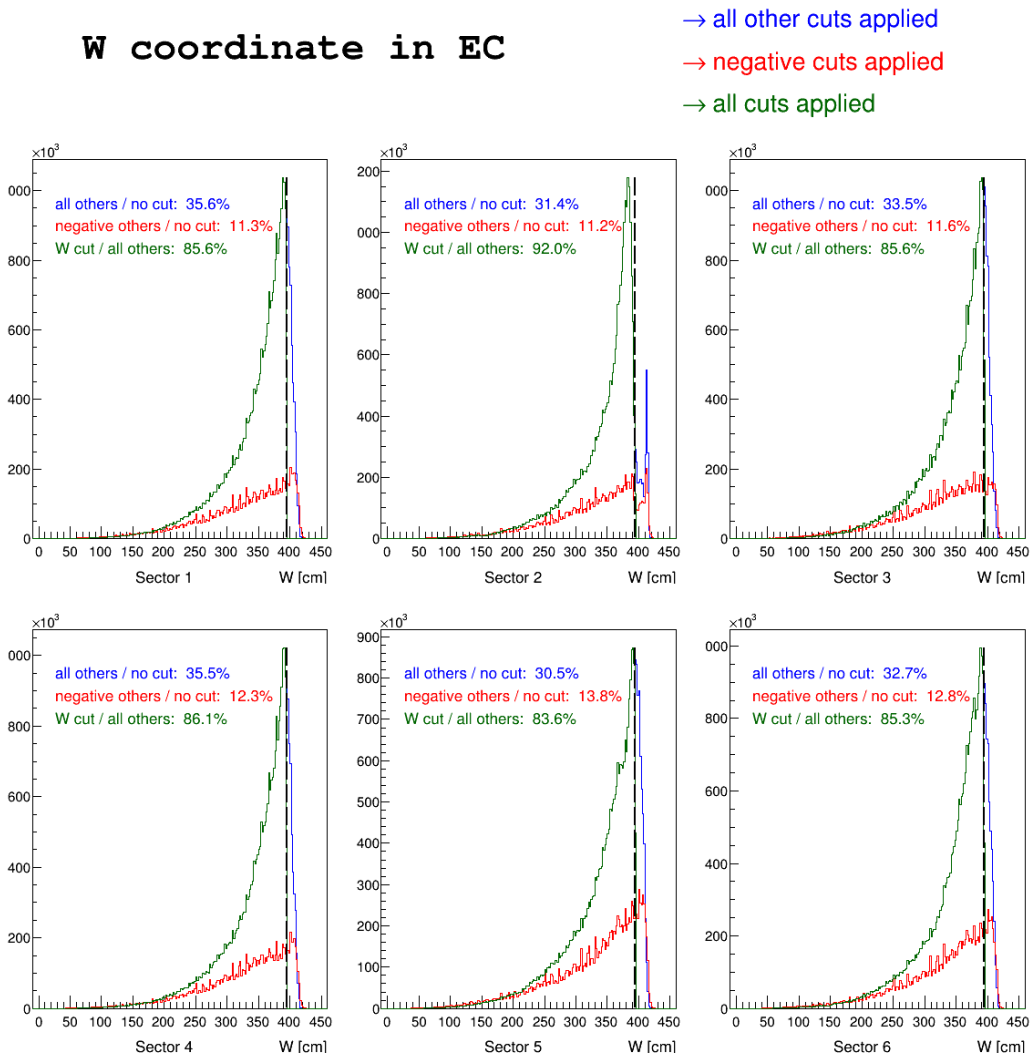

Figure 12: W track coordinate in the EC plane for all sectors. The cut is chosen to avoid edge effects that truncate the electron shower.

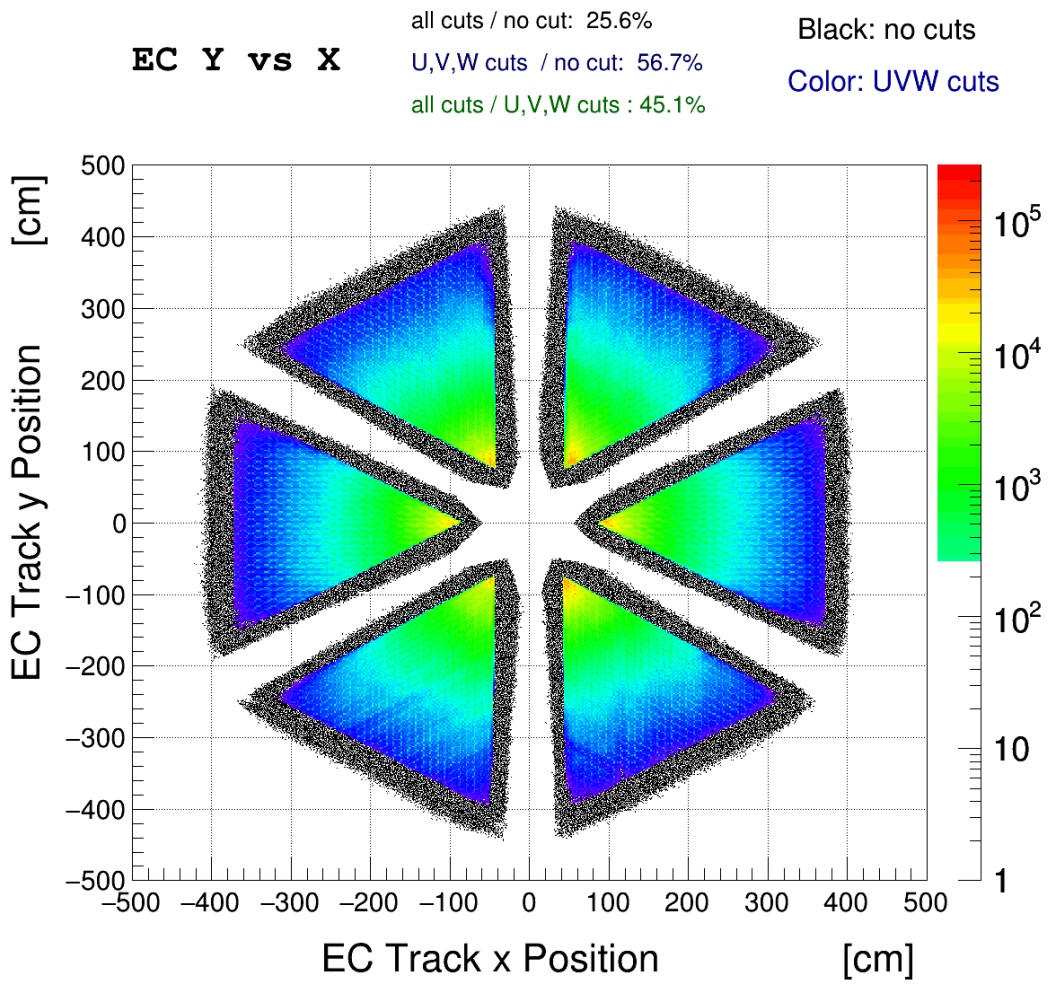

Figure 13: Y versus X track coordinate in the EC plane before and after the U, V, W cuts.

1.7 Minimum Ionizing Particles (MIP) rejection

The outer EC is 5/3 times bigger than the inner EC. Therefore pions, which do not shower and are minimum ionizing particles in the momentum range detected in CLAS, release a (small) quantity of energy in the outer and inner parts in the ratio 5 : 3, independent on their momentum.

In Fig. 14 the E_{out}/p versus E_{in}/p is shown for Sector 1. One can see the MIP signal along the $y = 5/3x$ line. Panel b. shows the same quantity when all other cuts are applied. One can see that the electron signal on the right. The cut is extrapolated by visually comparing panel a. and b. and trying to cut the most MIP as possible with a straight line $y = a + bx$. The line is sector dependent as shown in Fig. 15. This cut also include a minimum EC outer energy requirement of $1MeV$. The cut values used in each sector and their effectiveness are summarized in table 1.7.

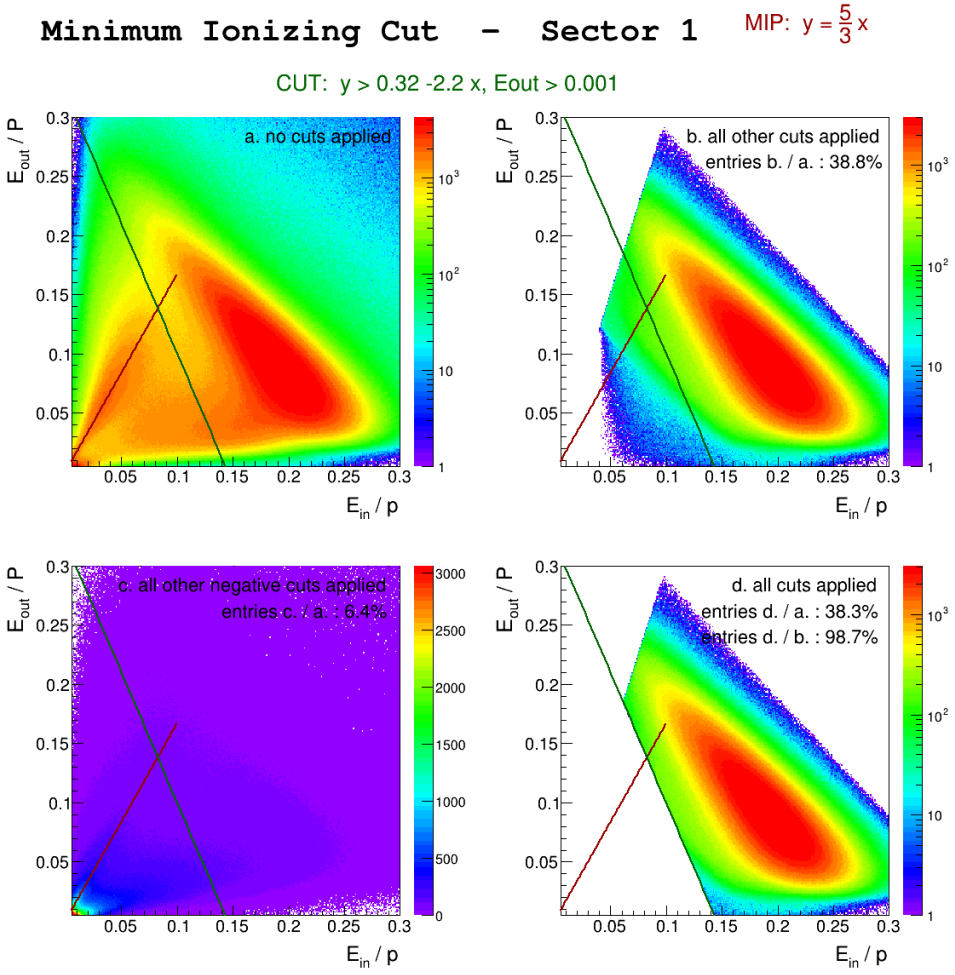

Figure 14: E_{out}/p versus E_{in}/p for Sector 1.

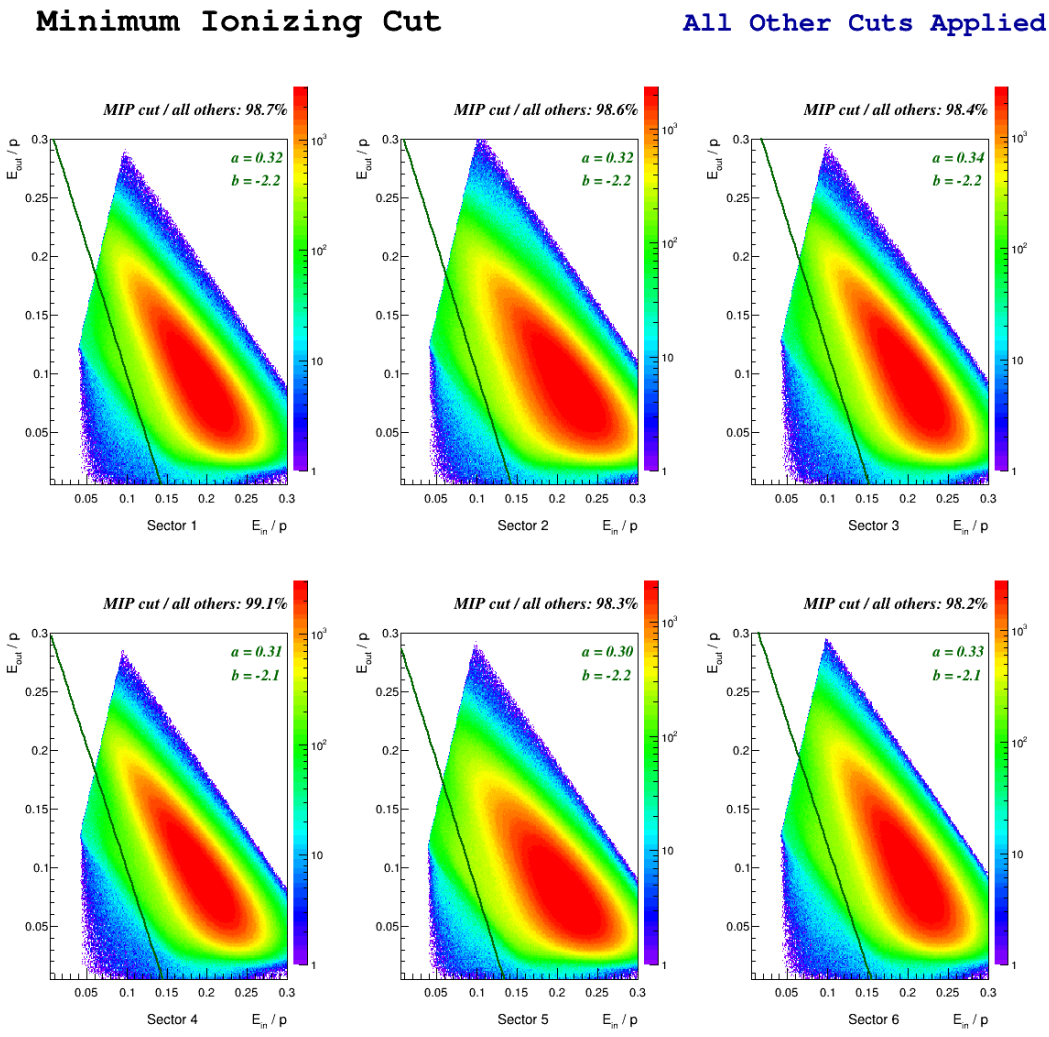

Figure 15: E_{out}/p versus E_{in}/p for all sectors. In every sector roughly 99 % of events with all other cuts applied also pass this cut.

Sector	y = a + bx pars	MIP cut / All others %	%
1	$a = 0.32$, $b = -2.2$	98.7	
2	$a = 0.32$, $b = -2.2$	98.6	
3	$a = 0.34$, $b = -2.2$	98.5	
4	$a = 0.31$, $b = -2.1$	99.1	
5	$a = 0.30$, $b = -2.2$	98.5	
6	$a = 0.33$, $b = -2.1$	98.3	

Table 3: The Minimum Ionizing cut values and effectiveness in each sector. The last column refers to events with signal in EC that pass the MIP cut.

1.8 Electromagnetic Shower Shape

Due to their shower shape, electrons release more energy in the inner part of the calorimeter than in the outer part. In fact the energy released in the inner part constitutes a good fraction of the total energy in the calorimeter. We chose to keep the events with

$$E_{in}/E_{TOT} \geq 0.25$$

This cut is very loose since most of the MIP are already cut out with all the other cuts, ass seen in Fig. 16. This cut keeps more than 99% of events in each sector.

1.9 Number of photo-electrons in the Čerenkov detector

In the past a threshold for the signal in the Čerenkov detector was necessary to eliminate electronic noise and the fact that negative pions produce Čerenkov light when their momentum is above ~ 2.5 GeV.

The ADC signal from the CC is converted in *number of photo-electrons* (nphe) and multiplied by 10. The number of photo-electrons detected in the Čerenkov Counter for electrons is typically between 5 and 20, or $10 \times nphe_{el} \sim 50 - 200$. You can see from Fig. 17 the $10 \times nphe$ distribution in each sector.

The peak at $nphe \sim 1$ represents not only background and negative pions, but good electrons with low CC efficency hits. For this reason it's better to apply the CC θ, ϕ and Timing match cuts.

In average (see Fig. 17) only $\sim 25\%$ of candidates pass the calorimeter cuts. If applied, the nphe cut would keep $\sim 90\%$ of them.

The *nphe* cut is chosen visually to be at the minimum of the *nphe* distribution between the background and electron signals peak.

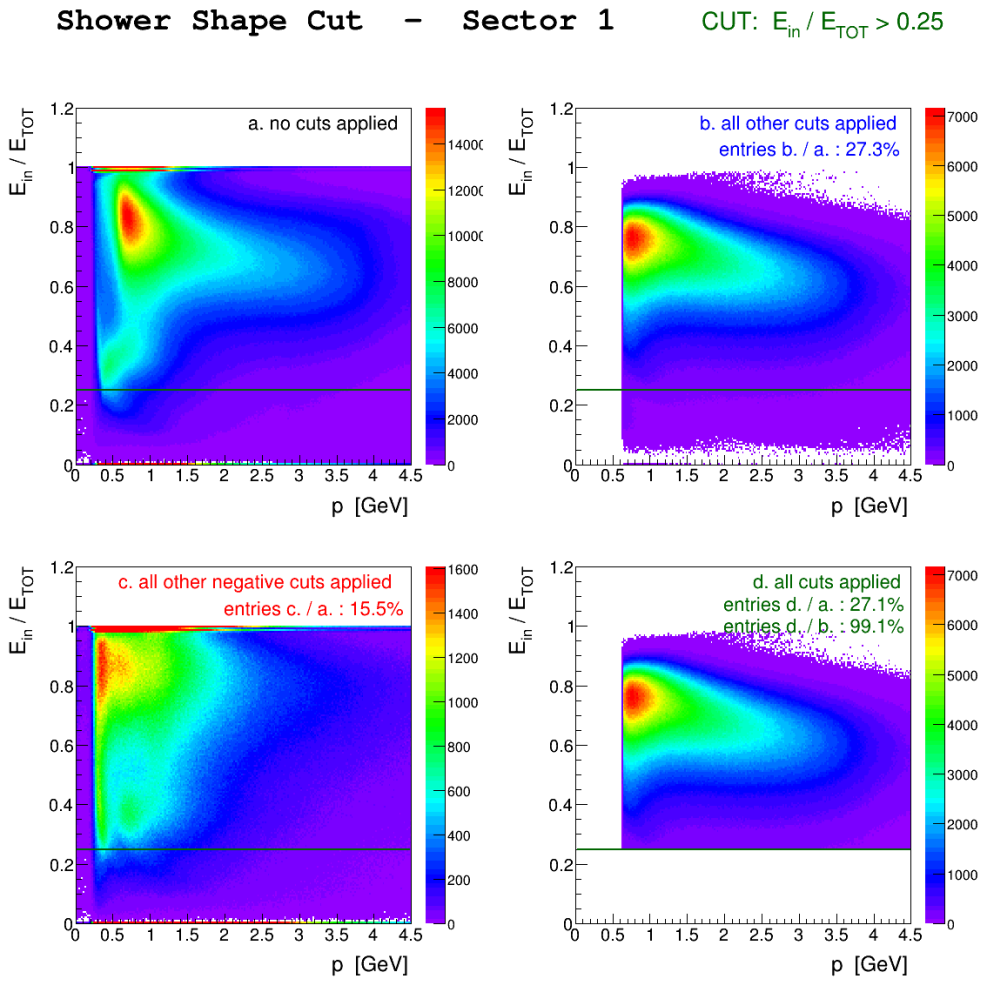

Figure 16: E_{in}/E_{TOT} for Sector 1. All other cuts (panel b.) almost completely rid of the MIP: 99.1% of those events are kept (Panel d.). Panel c. shows all other negative cuts except the minimum p cut.

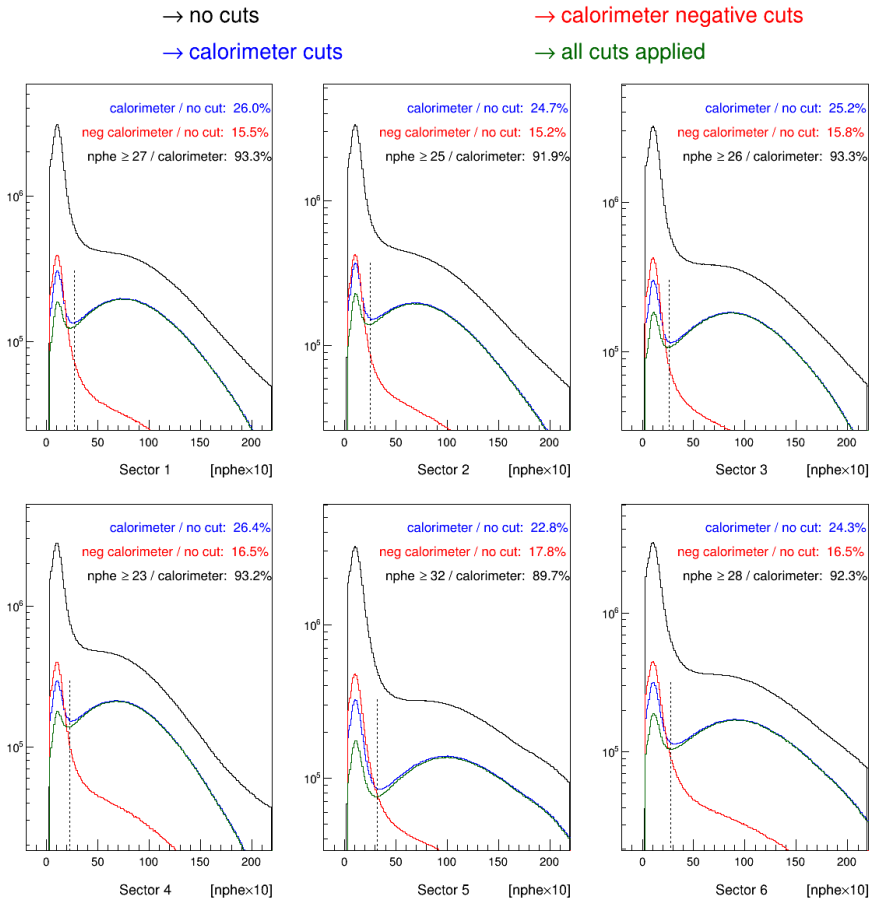

Figure 17: 10 × Number of photo-electrons distribution integrated over all sectors. In average, only $\sim 25\,\%$ pass the calorimeter cuts and of these, $\sim 90\,\%$ pass the *nphe* cut.

1.10 Summary of Electron Identification

In Fig. 18 a summary of the electron identifications cuts in all sectors is shown:

- Individual cuts effect: this is the percentage of events that would be selected by each individual cut if it was the only cut applied.
- Effectiveness: this is the percentage of events that are selected by each individual cut when all the other cuts are effective.
- Cumulative: this is the percentage of events that are selected by each individual cut when they are applied in the order show.

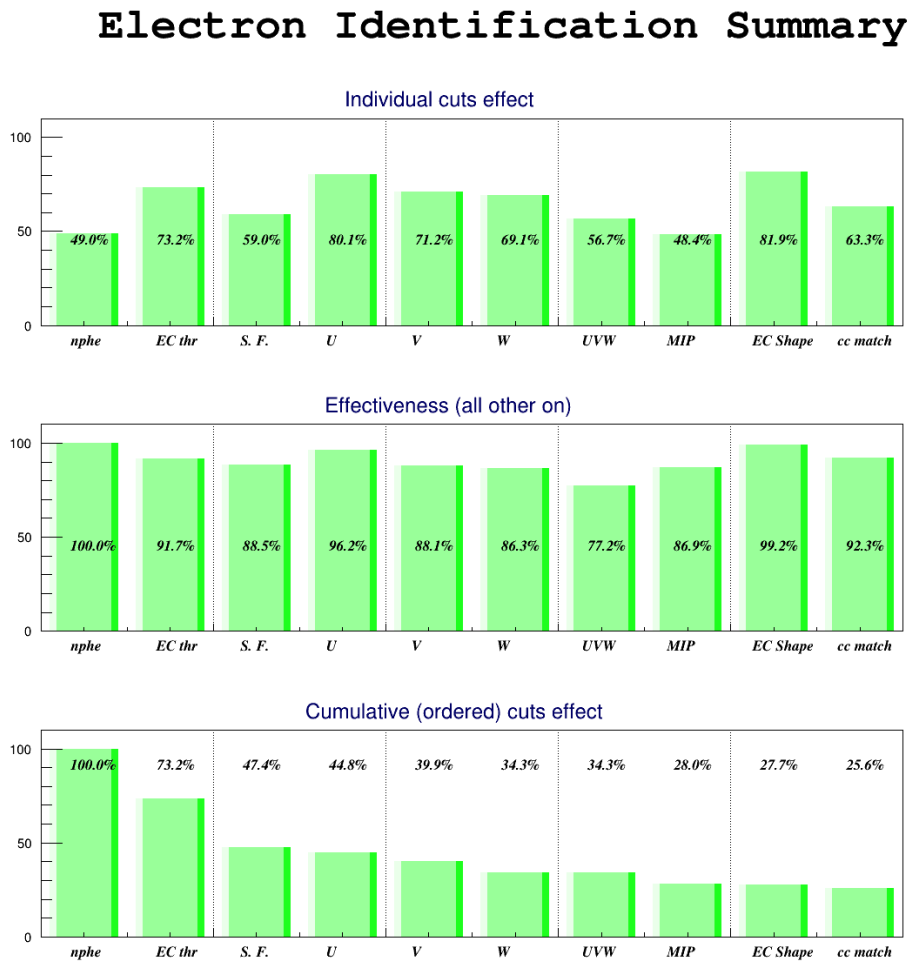

Figure 18: Electron Identification Summary. Top: effects of individual cuts. Middle: effectiveness of each cut. Bottom: effects of accumulated (ordered) cuts.

2 Proton identification

The purpose of this study is the proper identification of the scattered protons. The CLAS timing resolution decreases as the particles momentum increases. It is problematic to properly identify charged particles with the timing information alone at very large (greater than $3,4$ GeV) momentum. The goal of this analysis is to make the best possible selection of protons, while keeping in mind that further refinements based on individual reactions kinematics will be necessary.

2.1 CLAS Timing

During the event reconstruction the momentum of a track is calculated with the tracking procedure [10]. To determine its speed β, the start time T_0 is calculated as

$$T_0 = T_{el} - \frac{\ell}{c} - \frac{z - z_0}{c} \tag{2}$$

where T_{el} is the electron time from TOF measurement, ℓ is the path length of the electron track from the vertex to its TOF hit, c is the speed of light, z is the z-component of the event vertex and z_0 is the z position of the center of the target[1]. T_0 is then used as the reference for all the remaining tracks in the event. The track speed β is calculated as:

$$\beta = \frac{v}{c} = \frac{1}{c}\frac{\ell}{T - T_0} \tag{3}$$

where ℓ is the track path length from the target and T its TOF time. In Fig.19 is plotted β versus momentum for the all the particles after the electron particle ID. One can clearly see bands corresponding to pions, kaons, protons, deuterons.

2.2 ΔT cut

For this analysis every positive track (determined by its curvature in the torus field) is a *proton candidate*.

The difference ΔT between the time calculated using the candidates's momentum (assuming it is a proton) and its actual TOF time T should peak at zero for protons:

$$\Delta T = \frac{\ell}{\beta'} + T_0 - T(\sim 0) \tag{4}$$

where $\beta' = \sqrt{p^2/(M_P^2 + p^2)}$ is the speed of the track calculated from its momentum and M_P is the proton mass. A plot of ΔT versus momentum for Sector 1 is shown in Fig.20. The distribution is sliced along ΔT and each slide is fitted with 2 Gaussians + 2^{nd} order polynomial function to calculate the mean positions μ and sigmas σ of the proton and pions/kaons signals. The proton's μ and σ are then fitted with a 5^{th}-order polynomial. An example of μ fit is also shown in Figures 20 and 21.

At low momentum the protons are well separated. The pions distribution start to contaminate the protons when $\mu_P + 3\sigma_P < \mu_\pi - 3\sigma_\pi$; in that case $(\mu_\pi - 3\sigma_\pi - \mu_P)/3$ is used as the signal σ instead of σ_P. In Fig.21 the cuts for all sectors are shown.

Two quantities normally used to monitor the quality of the charged particles selection are β and the TOF Mass M^2_{TOF}:

$$M^2_{TOF} = \frac{p^2(1-\beta^2)}{\beta^2}$$

[1] For this experiment $z_0 = -4$ cm.

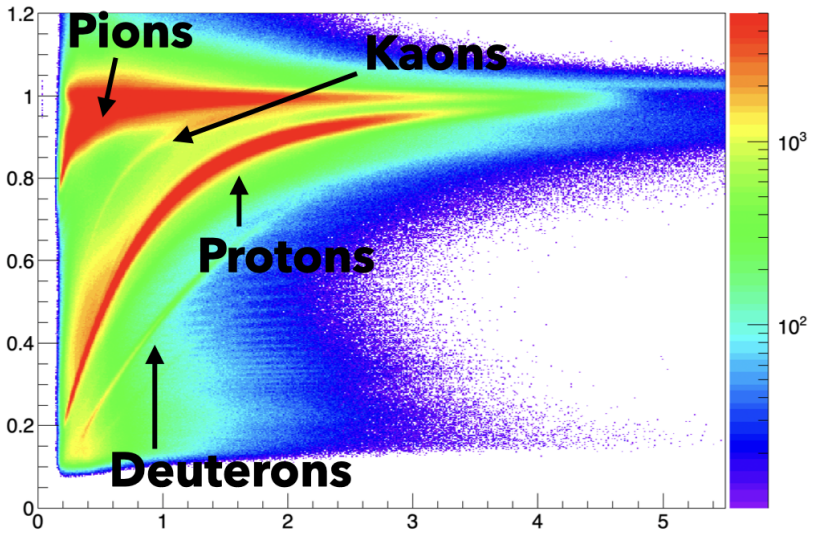

Figure 19: β versus momentum for positive particles in e1-6 running period. Bands corresponding to pions, kaons, protons and deuterons are visible.

Both β and M^2_{TOF} versus momentum are shown for sector 5 in Fig.22. The M^2_{TOF} was initially considered to perform this identification. However, when sliced, the corresponding 1-dimensional plots could not resolve the protons and kaons/pions signal as well as ΔT can.

The value of the μ and σ parameters used are listed in sec2.2.1.

2.2.1 Cut parameters

$$f(p) = a + bp + cp^2 + dp^3 + ep^4 + fp^5$$

	S1	S2	S3	S4	S5	S6
mean:						
a:	-0.9113	-0.655048	-0.904261	-0.709094	-0.724329	-0.418643
b:	2.98931	1.38425	1.76954	0.591925	4.06097	0.781139
c:	-4.09545	-2.10418	-1.9409	0.272274	-5.8547	-0.943656
d:	2.19893	1.2356	0.948967	-0.454383	3.18819	0.501819
e:	-0.495131	-0.290715	-0.194741	0.158209	-0.720678	-0.117491
f:	0.0389196	0.0232255	0.0136907	-0.0165409	0.0568144	0.00959472
sigma						
a:	6.16714	6.60215	5.87269	5.90242	5.96331	5.99657
b:	-12.1628	-14.4183	-10.6575	-11.7175	-12.2304	-12.4064
c:	9.86015	12.6391	8.00035	9.75136	10.391	10.69
d:	-3.74511	-5.02972	-2.86622	-3.90726	-4.04935	-4.35567
e:	0.679294	0.926557	0.497855	0.750446	0.737621	0.835659
f:	-0.0470408	-0.0639353	-0.033369	-0.0545215	-0.0505353	-0.0600134

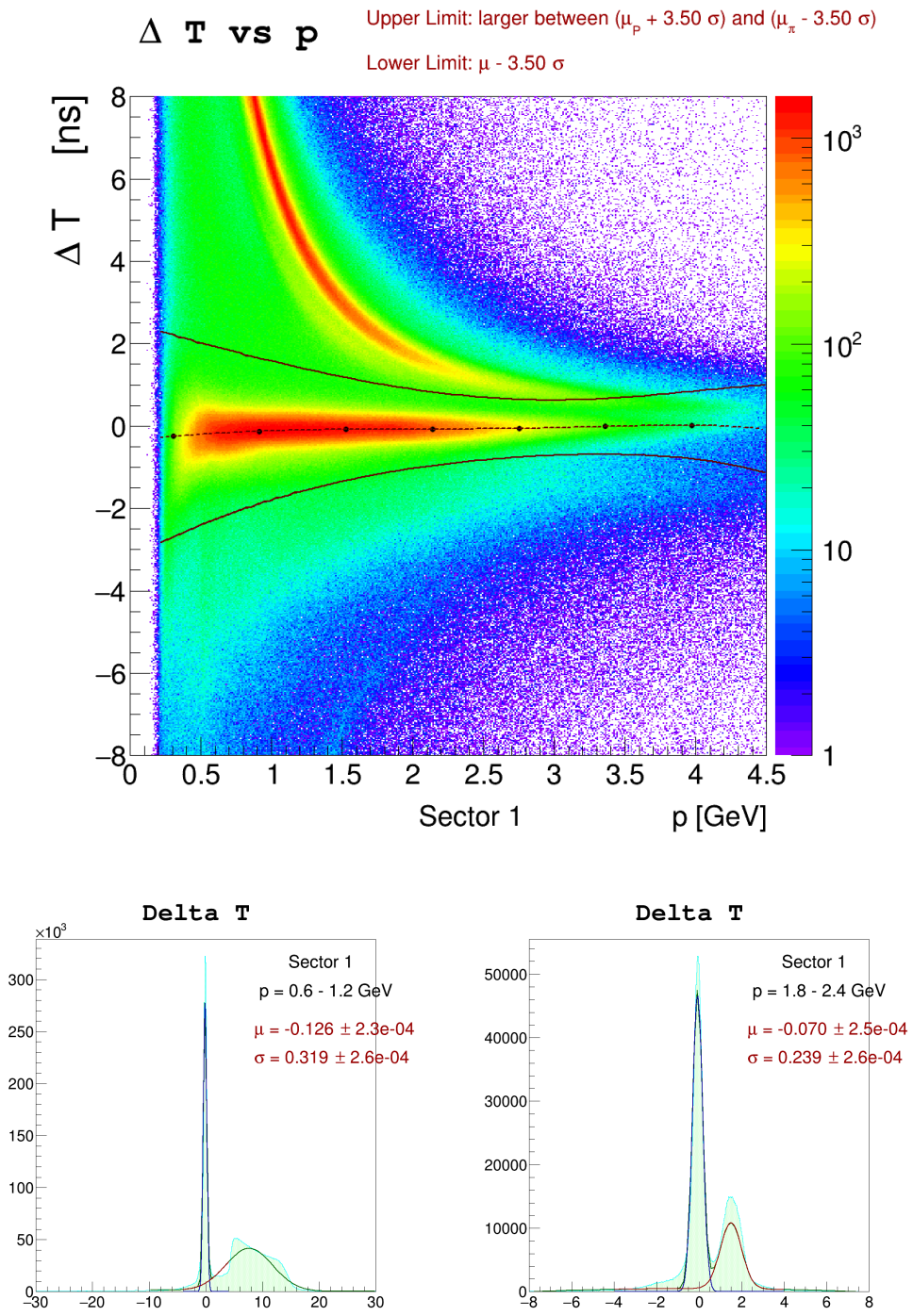

Figure 20: ΔT versus momentum and slices at different momentum. At low momentum the proton signal is well separated from kaons and pions, so we include everything up to 3σ from the pion/kaons signal. At high momentum kinematic constrains for exclusive channels will be necessary. The colors are as follows: blue: proton signal (gaussian). Red: pion signal (gaussian) + background (2^{nd} order polynomial). Dark green: total fit function.

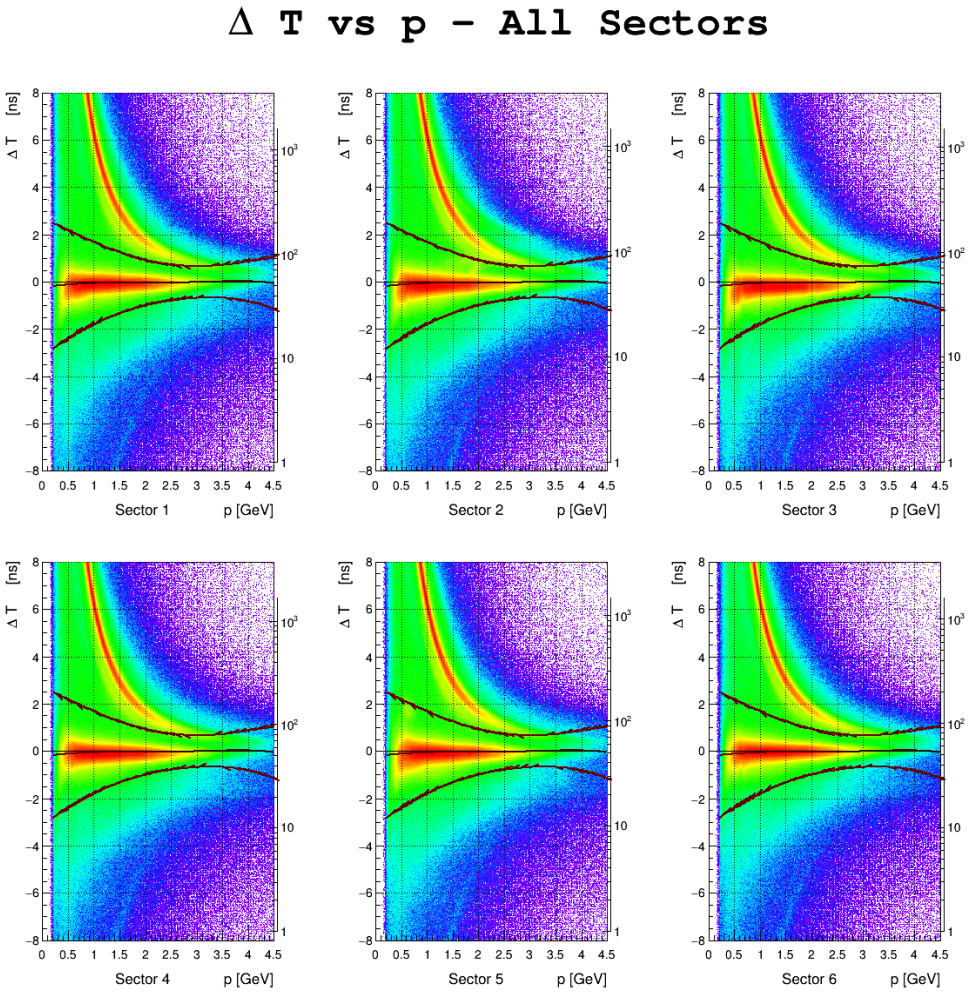

Figure 21: ΔT versus momentum cuts in all sectors. Plot grids emphasize the differences between sectors.

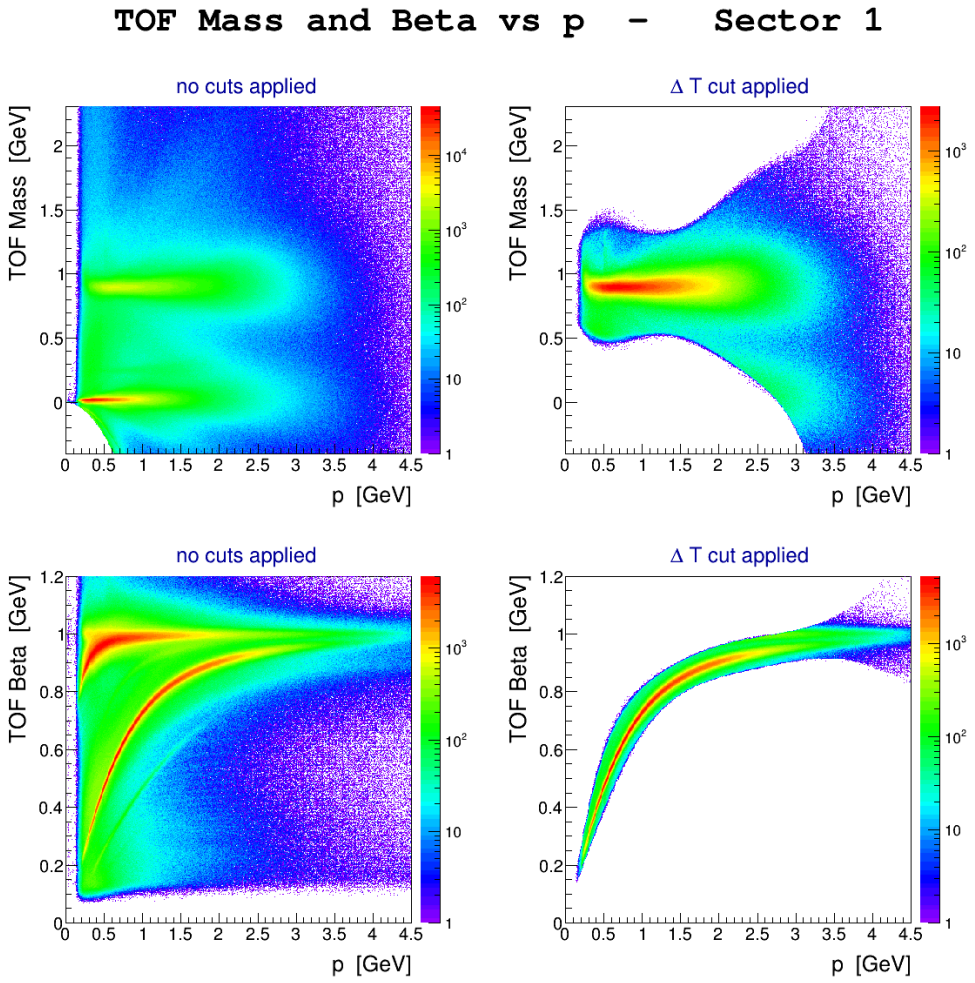

Figure 22: Left: β and M^2_{TOF} versus momentum for positive tracks with no cut applied. Right: the same quantities with the ΔT cut applied.

3 Vertex Correction, Selection

In the reconstruction software the track vertex (x, y, z) is calculated from its intersection with the sector midplane[2] of the corresponding sector. This procedure involve the assumption that the beam is centered along the z-axis. During the e1-6 experiment however the beam was not centered at $(x, y) = (0, 0)$ thus a sector-dependent offset is introduced in the vertex calculation.

3.1 Beam Offset

The displacement of the beam can be seen in Fig. 23, where the events on the window[3] downstream of the target were selected to fix the z position as reference. The calculated displacement [12] for the beam position is:

$$\begin{aligned} x_0 = &\quad 0.090 \quad cm \\ y_0 = &\quad -0.345 \quad cm \end{aligned}$$

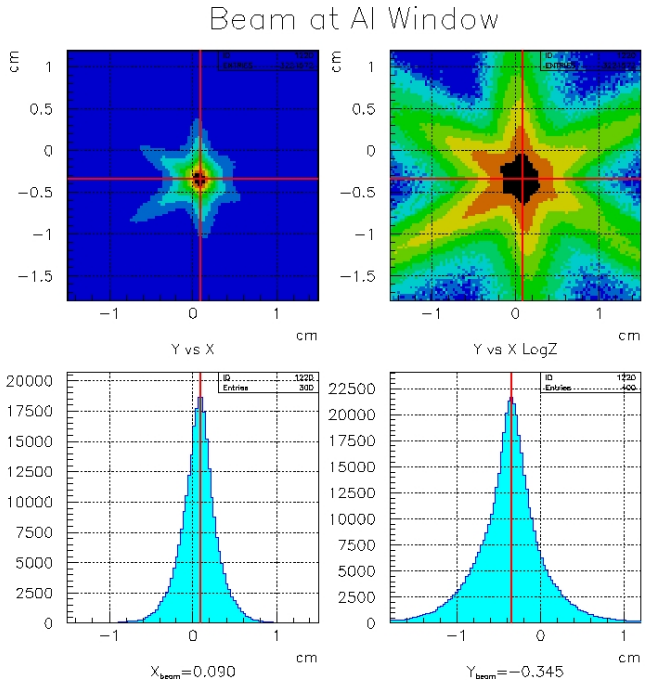

Figure 23: Top: y versus x position of the vertex at the window. Upper right: same as upper left, except plotted logarithmically. One can see that the beam spot was slightly shifted from $(0, 0)$. Bottom: the x (left) and y (right) distributions which led to the calculation: $(x_0, y_0) = (0.09, -0.345)cm$

[2]The midplane of a sector is defined by the plane that divide that sector in half and contains the beamline $(0, 0, z)$.

[3]A window was placed at $z = +0.5$ cm to help these kind of studies and to be a z-position reference.

3.2 Vertex Correction, Cut

To correct the vertex position it is sufficient to shift the midplanes so that they contain the correct beamline $(0.09, -0.345, z)$ and recalculate the intersection of the tracks with the new planes. This is illustrated in Fig.24.

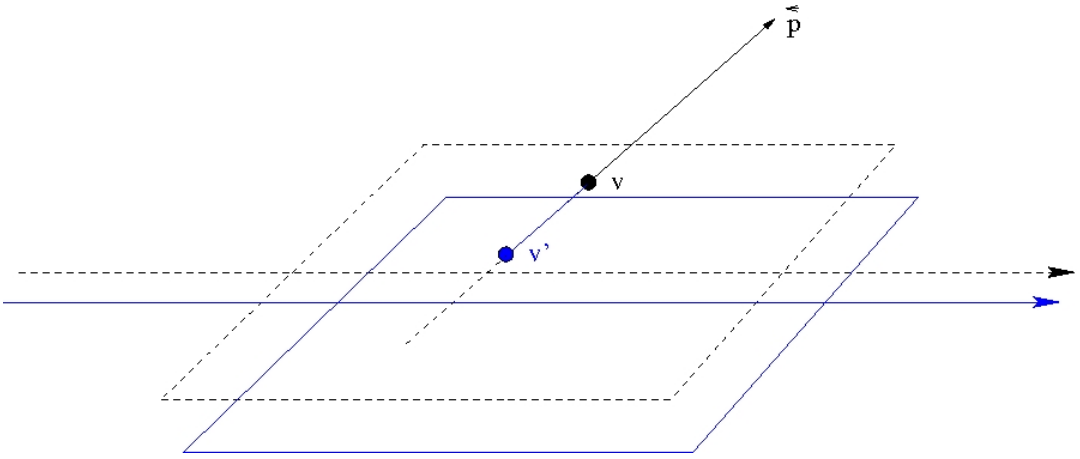

Figure 24: The vertex correction. The dashed plane is the original midplane containing the wrong beamline $(0, 0, 0)$. The point v is the intersection of the track (straight line along momentum $\vec{p}$) with this plane. The solid blue plane represents the corrected midplane containing $(0.09, -0.345, z)$. The correction algorithm simply intersects the same track with the corrected midplane.

The effect of the correction on the electrons and protons z position is shown in Fig. 25. After this correction, the vertex position resolution is good enough to introduce a cut on the z vertex of electron and protons in order to select events inside the target cell as follows:

$$-8\,cm \leq z \leq -0.8\,cm \tag{5}$$

The electron and proton vertices are also required to be coincident along the z axis within the reconstruction resolution, so an additional cut on $\Delta z = z_{electron} - z_{proton}$ is applied:

$$|\Delta z| < 3\,cm \tag{6}$$

The effect of the corrections and the values of the cuts are illustrated in Fig. 25 and Fig. 26.

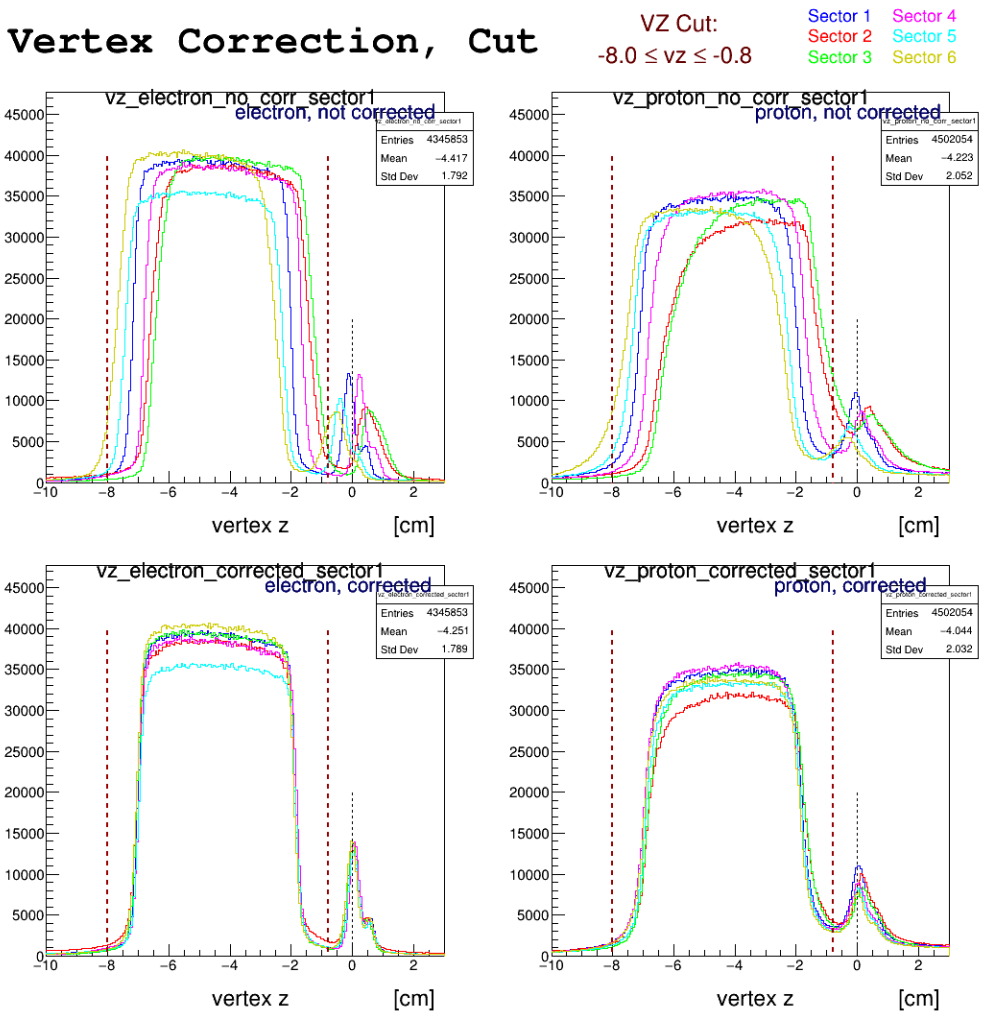

Figure 25: The effect of the correction on the electrons and protons z distributions for each sector. Top row: electron and proton z vertices, uncorrected. Bottom row: same distributions after the vertex correction. Vertical red lines: cuts of eq.5.

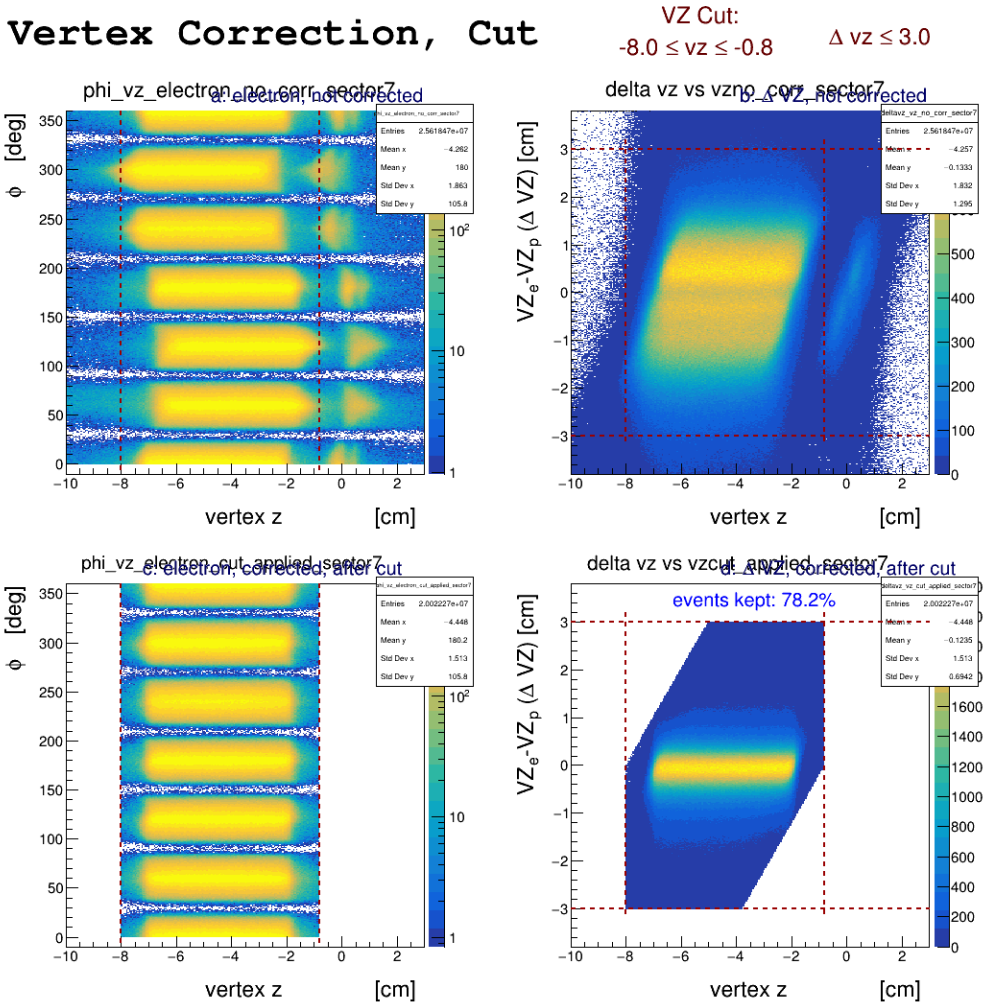

Figure 26: Top left: Δz versus $\phi_{electron}$, uncorrected. The typical sinusodial behaviour as a function of sector is indicative of the beam displacement. Bottom left: same distributions, after the vertex correction. Top right: Δz versus $VZ_{electron}$, uncorrected. Bottom right: same distributions, after the vertex correction. Vertical red lines: cuts of eq.5. Horizontal red lines: cuts of eq.6.

References

[1] K.S. Egiyan, *CLAS NOTE 99 - 007*

[2] S. Stepanya, *Private Communication*

[3] M. Osipenko, A. Vlassov and and M. Taiuti *CLAS NOTE 04 - 020*

[4] F.X. Girod, P. Khetarpal, *Private Communication*

[5] M. Osipenko, *Private Communication*

[6] M.D. Mestayer et al., The CLAS Drift Chamber System *Nucl. Inst. and Meth. A 449, 81 (2000)*

[7] E.S. Smith et al., The Time-of-Flight System for CLAS, *Nucl. Inst. and Meth. A 432, 265 (1999)*

[8] M. Amarian et al., The CLAS Forward Electromagnetic Calorimeter, *Nucl. Inst. and Meth. A 460, 239 (2001).*

[9] G. Adams et al., The CLAS Cerenkov Detector, *Nucl. Inst. and Meth. A 465, 414 (2001).*

[10] B. Niczyporuk, *CLAS NOTE 91 - 001*

[11] E.S. Smith et al., The Time-of-Flight System for CLAS, *Nucl. Inst. and Meth. A 432, 265 (1999)*

[12] Valeri Koubarovski, *Private Communication.*